Fermilab Library
0 1160 0061306 1
MAR 27 1998

DPNU-97-21
April 1997
typeset using JPSJ.sty <ver.0.8>

Electromagnetic Fields in Nonlinear Magnetosonic Waves with Relativistic Propagation Speeds

Shinji NAKAZAWA and Yukiharu OHSAWA

Department of Physics, Nagoya University, Nagoya 464-01

(Received April 2, 1997)

The structure of nonlinear magnetosonic waves with relativistic propagation speeds is studied through theory and particle simulation. First, the maximum values of magnetic and transverse electric fields and electric potential are analytically obtained as a function of the Alfvén speed and Mach number, under the assumption that waves propagate nearly steadily in the direction perpendicular to a magnetic field. Then, one-dimensional, relativistic, electromagnetic particle code with full ion and electron dynamics is used to study relativistic magnetosonic waves. It is found that the ion currents parallel to the the wave front become comparable to the electron currents in magnitude. As the propagation speed is increased, transverse fields become dominant components in electromagnetic fields of a wave. The theoretically obtained values of field quantities are in good agreement with the simulation results.

KEYWORDS: nonlinear magnetosonic waves, relativistic propagation speed, strong magnetic field

§1. Introduction

Nonlinear magnetosonic waves have been studied since the early age of plasma physics. Already in 1958, exact, finite-amplitude, stationary solutions were found.[1-3] In the solitary wave solution, the maximum magnetic field B_m is related to the field B_0 in the far upstream region as

$$B_m/B_0 = 2M - 1, \tag{1}$$

where M is the Alfvén Mach number; for a stationary solution, it must be in the range $1 < M < 2$. In the 1960's, Korteweg-de Vries (KdV) equations for perpendicular[4] and oblique[5,6] waves were obtained. These studies were based on nonrelativistic treatment. In addition, charge neutrality was assumed. Particle simulations were also performed to study shock structure, plasma heating, and particle acceleration.[7-10]

It was then pointed out that relativistic effects become important when the magnetic fields are rather strong, i.e., when the electron cyclotron frequency ω_{ce} is comparable to or greater than the electron plasma frequency ω_{pe}.[11-13] If the ratio ω_{ce}/ω_{pe} is in the range $1 \lesssim \omega_{ce}/\omega_{pe} \ll (m_i/m_e)^{1/2}$,

DPNU-97-21

where m_i is the ion mass and m_e is the electron mass, then the wave propagation speed is much smaller than the speed of light c (the Alfvén speed v_A is given by $v_A/c = (m_e/m_i)^{1/2}\omega_{ce}/\omega_{pe}$). Nevertheless, the electron (fluid) velocity parallel to the wave front can be close to c in the pulse region. It was also shown that the charge neutrality breaks down for large-amplitude waves when the ratio ω_{ce}/ω_{pe} is much greater than unity.

In a plasma with extremely strong magnetic field such as around a pulsar, the ratio ω_{ce}/ω_{pe} is much greater than unity. Even in coronal magnetic tubes in the Sun, its value can be of the order of ten, and the propagation speeds of nonlinear magnetosonic waves with high Mach numbers can be close to the speed of light. For such high-speed and large-amplitude magnetosonic waves, exact stationary solutions may not exist, and little work has been done.

In this paper, through theory and simulation, we study large-amplitude magnetosonic waves with relativistic propagation speeds. In §2, using a relativistic two-fluid model, and assuming that a nonlinear pulse propagates nearly steadily, we obtain maximum values of the magnetic field, transverse electric field, and electric potential as a function of the propagation speed and Alfvén speed. In §3, we carry out relativistic particle simulations. It is found that theoretically obtained values of electromagnetic fields are in good agreement with simulation results. It is also shown that, as the propagation speed is increased, electrostatic effects become less important; that is, the ratio of the longitudinal electric field component to transverse component (magnetic or transeverse elctric fields) become smaller. Furthermore, the the ion currents parallel to the wave front, which are negligible in magnetosonic waves in weak magnetic fields,[11] become comparable to the electron ones in magnitude. §4 gives a summary of our work.

§2. Nonlinear Structure

In this section we analytically discuss magnetosonic waves propagating perpendicular to a magnetic field, using a two-fluid model:

$$\frac{\partial n_j}{\partial t} + \nabla \cdot (n_j \boldsymbol{v}_j) = 0, \tag{2}$$

$$m_j \left(\frac{\partial}{\partial t} + (\boldsymbol{v}_j \cdot \nabla)\right)(\gamma_j \boldsymbol{v}_j) = q_j \boldsymbol{E} + \frac{q_j}{c}\boldsymbol{v}_j \times \boldsymbol{B}, \tag{3}$$

$$\frac{1}{c}\frac{\partial \boldsymbol{B}}{\partial t} = -\nabla \times \boldsymbol{E}, \tag{4}$$

$$\frac{1}{c}\frac{\partial \boldsymbol{E}}{\partial t} = \nabla \times \boldsymbol{B} - \frac{4\pi}{c}\sum_j q_j n_j \boldsymbol{v}_j, \tag{5}$$

$$\nabla \cdot \boldsymbol{E} = 4\pi \sum_j q_j n_j, \tag{6}$$

where the subscript j refers to ions (j =i) or electrons (j =e); m_j is the mass, q_j the charge, n_j the number density, $\boldsymbol{v}_j$ the velocity, and γ_j the Lorentz factor.

We assume that the waves propagate in the x direction in a magnetic field that points in the z direction. Hence the field quantities B_x, B_y, and E_z can be set to be zero. The velocities in the z direction are constant in time and are taken to be zero.

The phase velocity of the linear magnetosonic wave is given by

$$v_{\rm p} = v_{\rm A}/[1 + (v_{\rm A}/c)^2]^{1/2}, \tag{7}$$

in the long-wavelength limit, where the Alfvén speed $v_{\rm A}$ is defined as

$$v_{\rm A}^2 = B_0^2/(4\pi m_{\rm i} n_0). \tag{8}$$

The subscript 0 denotes equilibrium quantities.

If the Alfvén speed is quite high and the wave amplitude is large, we do not expect that there are exact stationary solutions, for which we can assume that in the wave frame the time derivatives are exactly zero at any place, $\partial/\partial t = 0$. In fact, particle simulations[12] show that, when the magnetic fields are rather strong, i.e., $\omega_{\rm ce} \gtrsim \omega_{\rm pe}$, a large-amplitude pulse emits small-amplitude pulses which propagate faster than the original pulse. Such a system is not exactly stationary.

However, if the amplitudes of emitted pulses are small, then their effects on the original pulse would also be small. We therefore assume that a large-amplitude magnetosonic pulse can propagate nearly steadily. Its velocity will be designated by $v_{\rm sh}$ (the subscript sh stands for a shock wave); $v_{\rm sh}$ can be close to the speed of light c. Hence in the frame that moves with the same velocity as the main pulse we can assume that $\partial/\partial t \simeq 0$ (we will call this system the wave frame).

Then, from the continuity equation, it follows that

$$n_j v_{jx} = n_{\rm w0} v_{\rm w0} = \text{constant}, \tag{9}$$

where $n_{\rm w0}$ and $v_{\rm w0}$ $(= -v_{\rm sh})$ are the density and velocity, respectively, in the far upstream region in the wave frame. Multiplying the x component of eq. (3) by n_j and adding over the particle species, we have

$$\sum_j m_j n_j v_{jx} \frac{d}{dx}(\gamma_j v_{jx}) = \sum_j \left(q_j n_j E_x + \frac{q_j n_j}{c} v_{jy} B \right), \tag{10}$$

where B is the z component of the magnetic field. Then, using eqs. (5), (6), and (9), we obtain

$$\frac{d}{dx}\left(\sum_j m_j \gamma_j n_{j\rm w0} v_{j\rm w0} v_{jx} + \frac{B^2 - E_x^2}{8\pi} \right) = 0. \tag{11}$$

Because $v_{\rm ix}$ and $v_{\rm ex}$ are of the same order, we can neglect the terms proportional to the electron mass, $m_{\rm e}$. We thus have

$$m_{\rm i}\gamma_{\rm i}(x) n_{\rm w0} v_{\rm w0} v_{\rm ix}(x) + \frac{B(x)^2 - E_x(x)^2}{8\pi} = m_{\rm i}\gamma_0 n_{\rm w0} v_{\rm w0}^2 + \frac{B_{\rm w0}^2}{8\pi}. \tag{12}$$

Here γ_0 is defined as

$$\gamma_0 = [1 - (v_{\rm w0}/c)^2]^{-1/2}. \tag{13}$$

The right-hand side of eq. (12) is a quantity in the far upstream region. As in the nonrelativistic case,[1,2,11] we assume that the magnetic field and electric potential have thier maximum values at the same point (this will be confirmed later by simulations). Hence at this point the longitudinal electric field E_x becomes zero. Also, at this point, ion velocity in the x direction is much smaller than that in the far upstream region (this will also be shown by simulations); in the pulse region the velocity $v_{\rm ix}$ is decelerated by the electric potential and the strong magnetic field.[1,2,11] (This is not the case when the amplitude is very small; in small amplitude waves, values of $v_{\rm ix}$ in the pulse region must be close to those in the far upstream region.) We thus find the maximum value of the magnetic field in the wave frame as

$$\frac{B_{\rm wm}}{B_{\rm w0}} = \left(1 + \frac{m_{\rm i}\gamma_0 n_{\rm w0} v_{\rm w0}^2}{(B_{\rm w0}^2/8\pi)} \right)^{1/2}. \tag{14}$$

By virtue of the Lorentz transformation between the wave frame and laboratory frame (the quantities in the laboratory frame will be denoted by the subscript l)

$$B_{\rm w}(x_{\rm w}) = B_{\rm l}(x_{\rm l})/\gamma_0 + (\gamma_0 - \gamma_0^{-1}) B_{\rm l0}, \tag{15}$$

$$n_{\rm w0} = \gamma_0 n_{\rm l0}, \tag{16}$$

we have the maximum magnetic field in the laboratory frame

$$\frac{B_{\rm lm}}{B_{\rm l0}} = \gamma_0^2 \left(1 + \frac{2(\gamma_0^2 - 1)}{\gamma_0^2} \frac{c^2}{v_{\rm A}^2} \right)^{1/2} + 1 - \gamma_0^2. \tag{17}$$

As is evident from the derivation, this relation is not valid when the amplitude is quite small.

Also, from the Lorentz transformation

$$E_{\rm ly}(x_{\rm l}) = \gamma_0 [E_{\rm w0} - (v_{\rm sh}/c) B_{\rm w}(x_{\rm w})], \tag{18}$$

we obtain the maximum electric field in the y direction (parallel to the wave front) in the laboratory frame

$$E_{\rm lym} = (v_{\rm sh}/c) B_{\rm l0} (B_{\rm lm}/B_{\rm l0} - 1). \tag{19}$$

This relation is also satisfied in the exact stationary solution.[1,2,11] Substitution of eq. (17) in eq. (19) yields

$$E_{\rm lym} = (v_{\rm sh}/c) B_{\rm l0} \gamma_0^2 \left[\left(1 + \frac{2(\gamma_0^2 - 1)}{\gamma_0^2} \frac{c^2}{v_{\rm A}^2} \right)^{1/2} - 1 \right]. \tag{20}$$

Next, we will obtain the electric potential formed in a nonlinear pulse. The y component of eq. (5) (with $\partial/\partial t = 0$) reads

$$\frac{\partial B}{\partial x} = \frac{4\pi}{c}(e n_{\rm e} v_{\rm ey} - q_{\rm i} n_{\rm i} v_{\rm iy}). \tag{21}$$

The electron velocity parallel to the wave front, $v_{\rm ey}$, can be approximated by the drift velocity

$$v_{\rm ey} = -c E_x / B. \tag{22}$$

When the wave propagation speed is much lower than the speed of light, the electron velocity is much greater than the ion velocity.[11] $|v_{ey}| \gg |v_{iy}|$. For such a case, ion currents can be neglected, and eq. (21) can be written as

$$\frac{\partial B}{\partial x} = -4\pi e \frac{n_e}{B} E_x. \tag{23}$$

From Faraday's law, (4), and the continuity equation, (2), we find that the ratio n_e/B is constant:

$$\frac{n_e}{B} = \frac{n_{w0}}{B_{w0}}, \tag{24}$$

because the electron velocity in the x direction is given by

$$v_{ex} = cE_y/B. \tag{25}$$

The longitudinal electric field E_x is related to the electric potential through $E_x = -\partial\varphi/\partial x$. Equation (23) can therefore be integrated to give

$$e\varphi_{wm} = \frac{B_{w0}(B_{wm} - B_{w0})}{4\pi n_{w0}}, \tag{26}$$

where φ_{wm} is the maximum value of the potential in the wave frame. Because the electric potential in the laboratory frame can be given by

$$\varphi_l = \gamma_0 \varphi_w, \tag{27}$$

we obtain the maximum value of the potential in the laboratory frame

$$e\varphi_{lm} = m_i v_A^2 \left(\frac{B_{lm}}{B_{l0}} - 1\right). \tag{28}$$

In deriving eq. (28), we have neglected the ion currents in the direction parallel to the wave front. However, as will be shown by simulations in the next section, the ion currents can be comparable to the electron currents in magnitude for large-amplitude magnetosonic waves with relativistic propagation speeds. Therefore, to have a more accurate relation, we have to include effects of ion currents in Ampére's law; instead of eq. (23) we calculate the following equation

$$\frac{\partial B}{\partial x} = -4\pi \left(e\frac{n_e}{B}E_x + \frac{q_i n_i v_{iy}}{c}\right). \tag{29}$$

In the wave frame, ion speed ($\sim v_{sh}$) is quite high, of the order of the speed of light. Thus, in the pulse region where the magnetic field sharply rises, the ion motion is described by the gyro-motion with $E_{w0} \times B$ drift; when the speeds of gyration and of drift are equal, we have a cycloid. As in the motion of heavy ions in a magnetosonic pulse with a nonrelativistic propagation speed, [14] the longitudinal electric force is less important. When an ion particle enters the pulse region with $v_{ix} \simeq v_{sh}$, then v_{ix} is rapidly converted to v_{iy} by the Lorentz force. When v_{iy} becomes sufficiently large, this acceleration in the y direction ceases. Figure 1 shows a simlified schematic diagram of an ion orbit in the wave frame (see also a phase space plot in Appendix). For a particle motion

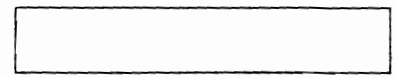

Fig. 1. Schematic diagram of an ion orbit in the (x, y) plane in the wave frame.

similar to a cycloid, eq. (29) can be integrated to give

$$\frac{e\varphi_{lm}}{m_i v_A^2} = \left(\frac{B_{lm}}{B_{l0}} - 1\right) - A\frac{2\gamma_0^4 (v_{sh}/v_A)^2}{(B_{lm}/B_{l0}) + 2\gamma_0^2 - 1}. \tag{30}$$

The quantity A is a numerical factor of the order unity (strictly speaking, it also depends on the amplitude). The details of the calculation are found in Appendix.

§3. Particle Simulation of Nonlinear Waves

To further discuss the propagation of large-amplitude magnetosonic waves in plasmas with high Alfvén speeds, we will use a one-dimension (one spatial coordinate and three velocity components), fully electromagnetic particle code with full ion and electron dynamics. The total grid size is $L_x = 1024\Delta_g$, where Δ_g is the grid spacing. All lengths and velocities in the simulations are normalized to Δ_g and $\omega_{pe}\Delta_g$, respectively, where ω_{pe} is the spatially averaged plasma frequency. The simulation particles are confined in the region $100 < x < 924$, being specularly reflected at $x = 100$ and $x = 924$. Outside the plasma region, electromagnetic radiation leaving the plasma region is absorbed; thus we can avoid the interactions between the left and right sides of the plasma regions through the vacuum region.[15] The momentum components $p_{j\sigma}$ ($\sigma = x$, y, or z) are initially distributed according to an isotropic Maxwellian with average momentum zero. However, for particles in the region $100 < x < 180$, the x-component of the momentum, p_{jx}, has a shifted Maxwellian distribution function with a positive average value; these particles act as a piston that pushes the neighboring plasma and excites a shock wave.[9]

The number of simulation particles are $N_i = N_e = 65536$. The ion-to-electron mass ratio is $m_i/m_e = 100$, and the light speed is $c = 4$. The electron and ion thermal velocities are $v_{Te} = 0.8$ and $v_{Ti} = 0.08$. The electron skin depth is $c/\omega_{pe} = 4$. The strength of the external magnetic field was chosen so that $\omega_{ce}/\omega_{pe} = 3.0$ or 5.0. For $\omega_{ce}/\omega_{pe} = 3.0$, the beta value, which is defined as the ratio of the plasma pressure to the magnetic energy, is $\beta = 0.019$, and the Alfvén speed is $v_A = 1.2$. The ion gyro-radius is $\rho_i = 2.7$. On the other hand, for $\omega_{ce}/\omega_{pe} = 5.0$, these values are $\beta = 0.0067$, $v_A = 2.0$, and $\rho_i = 1.6$.

The time step Δt was taken to be very small for each run. In the far upstream region, it was

$\omega_{ce}\Delta t \sim 0.02$. Even at a region of the strongest magnetic field, therefore, it was $\omega_{ce}\Delta t \lesssim 0.2$.

First, we show in Fig. 2 snapshots of a perpendicular magnetosonic pulse (quasi shock wave). From the top panel to the third one, plotted are the magnetic field B, transverse electric field E_y,

Fig. 2. Profiles of B, E_y, φ, and phase space plots (x, p_{jx}) and (x, p_{jy}) for ions and electrons.

and the electric potential φ at $\omega_{pe}t = 180$. The lower four panels show phase space plots (x, p_{jx}) and (x, p_{jy}) for the ions and electrons. In the figure, the quantities B, E_y, φ, and p_j are normalized to B_0, B_0, $m_i v_A^2/e$, and $m_j c$, respectively. Because in the simulations all the quantities are observed in the laboratory frame (except for Fig. 4), the subscript 1 is omitted. The field quantities B, E_y, and φ have similar profiles and have their maximum values at nearly the same point. As mentioned in the previous section, even though the magnetosonic pulse propagates nearly steadily, small-amplitude pulses are emitted from the main pulse and move away from it;[12] see the upper two panels.

This is a case with $\omega_{ce}/\omega_{pe} = 3.0$. If we define the Mach number M as the ratio of shock speed v_{sh} to phase velocity of linear magnetosonic wave v_p

$$M = v_{sh}/v_p, \tag{31}$$

then M is observed to be 2.8. Because $v_p/c = 0.29$, the speed ratio v_{sh}/c is 0.81, and the Lorentz factor for this speed ratio is $\gamma_0 = 1.7$.

Figure 3 shows spatial profiles of plasma current densities in the direction parallel to the wave front, j_y (normalized to the quantity $e\Delta_s^2\omega_{pe}$), at the same moment as Fig. 2; in the upper panel we show ion current density j_{iy} and electron current density j_{ey}, while in the lower one we show the total current density, $j_y = j_{iy} + j_{ey}$. Certainly, the magnitude of the ion current density is comparable to that of the electron current density in magnitude.

Figure 4 shows ion momenta p_{ix} in the wave frame. The vertical line at $x_w = 322$ represents the x position where the potential takes its maximum value, $x_w = x_{wm}$. The values of p_{ix} around this point are much smaller than those in the far upstream region. This ascertains the assumption that, in eq. (12), the first term on the right-hand side can be neglected at $x_w = x_{wm}$ compared to the first term on the left-hand side.

Fig. 3. Profiles of current densities parallel to the wave front. In the upper panel, the ion and electron current densities are shown. In the lower panel, the total current density is plotted.

Fig. 4. Ion momenta in the wave frame.

Here we obtained p_{ix} by the Lorentz transformation of the ion momenta p_{ix} at $\omega_{pe}t = 180$ in Fig. 2 in the laboratory frame. Thus the times at different x positions in Fig. 4 are not the same. However, the average value (fluid velocity) of p_{iwx} at $x_w = \infty$ is independent of time. Hence the difference between the average values of p_{iwx} at $x_w = x_{wm}$ and at $x_w = \infty$ should be independent of time, if the wave propagation is steady.

Carrying out simulations with different values of propagation speed of pulse, v_{sh}, we can observe the dependence of the magnetic field amplitude on the pulse speed v_{sh}; it is plotted in Fig. 5. The upper panel is for the case with $v_A/c = 0.3$ ($\omega_e/\omega_{pe} = 3.0$), while the lower one is for $v_A/c = 0.5$ ($\omega_e/\omega_{pe} = 5.0$). The circles and triangles show simulation results measured at around $\omega_{pe}t \simeq 120$ and at $\omega_{pe}t \simeq 180$, respectively. The solid lines are the theoretical prediction given by eq. (17). The dotted lines are the nonrelativistic theory given by eq. (1); even though this equation is not applicable to these parameters, for comparisons, we extrapolated the theory. In both the new theory and simulation results, the maximum value B_m/B_0 rapidly increases with Mach number M (or the propagation speed v_{sh}) in the high Mach number region.

In Fig. 6 are shown maximum values of the transverse electric field E_y as a function of the pulse speed v_{sh} (or the Mach number M). As in the previous case, the Alfvén speed in the upper panel is $v_A/c = 0.3$, and that in the lower panel is $v_A/c = 0.5$. The circles and triangles are simulation results at $\omega_{pe}t \simeq 120$ and at $\omega_{pe}t \simeq 180$. Also, the solid lines are theoretical prediction, eq. (20). For both the magnetic and the transverse electric fields, the theory and simulation are in good

Fig. 5. Magnetic field amplitude versus pulse speed. The Alfvén speed is $v_A/c = 0.3$ for the upper panel and is $v_A/c = 0.5$ for the lower panel. The circles and triangles show simulation results. The solid lines are theoretical prediction. The dotted lines are extrapolation of nonrelativistic theory.

agreement.

Fig. 6. Amplitude of transverse electric field as a function of the pulse speed.

Figure 7 shows maximum values of the electric potential as a function of the pulse speed v_{sh} (or the Mach number M). The dotted lines are the theory neglecting the ion currents, which gives larger values than the observations. The solid lines are the theory including ion currents. The theory taking ion currents into account gives a better fit than the theory without ion currents. This is consistent with the direct observations of plasma currents shown in Fig. 3.

Fig. 7. Electric potential versus pulse speed.

We show in Fig. 8 how the amplitude ratios change as a function of the pulse speed v_{sh}; the ratios $E_{ym}/(B_m - B_0)$ and $E_{xm}/(B_m - B_0)$ are plotted. The open and closed circles are simulation results for E_{ym} and E_{xm}, respectively. The thick straight line represents the theory, eq. (19). As the

theory predicts, the amplitude ratio $E_{ym}/(B_m - B_0)$ increases with pulse speed. However, the ratio of the longitudinal electric field to the magnetic field, $E_{xm}/(B_m - B_0)$, decreases with increasing pulse speed. As the pulse speed increases, the transverse fields, E_y and B, become the dominant components in electromagnetic fields in a shock wave.[16]

Fig. 8. Amplitude ratios $E_{ym}/(B_m - B_0)$ and $E_{xm}/(B_m - B_0)$ as a function of the pulse speed. The straight line is the theory for E_{ym}.

§4. Summary

Through theory and particle simulation, we have studied the structure of a large-amplitude magnetosonic wave propagating perpendicular to a magnetic field with a relativistic speed. First, on the basis of the relativistic two-fluid model, we analytically obtained the strengths of magnetic and transverse electric fields and the magnitude of electric potential in a nonlinear pulse, assuming that the pulse propagates nearly steadily; the charge neutrality was not assumed. Then, using a one-dimensional, relativistic, electromagnetic particle code with full ion and electron dynamics, we investigated the propagation of large-amplitude magnetosonic waves in plasmas with high Alfvén speed; the propagation speeds of shock waves we studied were $0.5 \lesssim v_{sh}/c \lesssim 0.9$. It was found that the magnitudes of electromagnetic fields obtained from the theory are in good agreement with the simulation results. Also, both theory and simulation show that the transverse components (magnetic and transverse electric fields) become predominant over the longitudinal ones when the magnetosonic waves have highly relativistic propagation-speeds.

Unlike the weak magnetic field case, the ion currents parallel to the wave front are comparable to the electron currents in magnitude. The theory including the ion currents gives potential values closer to simulation results than the theory neglecting the ion currents.

The ion currents were obtained from simple physical considerations. Thus further investigation on the ion motions is desirable to obtain more accurate ion currents and potential in large-amplitude magnetosonic waves with relativistic speeds. The investigation of ion orbits is also needed to develop the research of particle acceleration in strong magnetic fields.

Acknowledgements

The authors are grateful to Dr. Mieko Toida for stimulating discussions. This work was supported in part by the US-Japan Joint Institute for Fusion Theory.

Appendix: Estimation of Ion Current

It is quite difficult to accurately and rigorously estimate the ion currents in the pulse region; to do this we need to know precise information of ion motions. Here we will obtain the ion currents from a simple physical picture; our treatment will not be fully relativistic. Figure 9 shows a snapshot of ion phase space (x, v_y) obtained from a particle simulation; the simulation parameters are the same as those in Fig. 2. From this, we see that, when the ions penetrate the pulse region, v_y increases

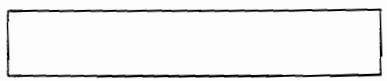

Fig. 9. Ion phase space plot (x, v_y).

up to a certain maximum value; next it quickly decreases to a negative maximum value and then becomes zero. Thus in the (x, y) plane in the wave frame, the ion orbits can be schematically drawn as in Fig. 1.

For a large-amplitude magnetosonic wave with a relativistic speed, the ion velocity is quite high (much higher than the thermal speed) in the wave frame. Also, the magnetic field is strong in the pulse region. Hence, the ion motion is similar to a cycloid; gyro-motion with $E_{y0} \times B$ drift, which is consistent with the motion shown in Figs. 1 and 8. That is, the ion velocity is given by

$$v_x - cE_{y0}/B = v_\perp \cos(-\omega_{ci}t + \pi), \tag{A·1}$$

$$v_y = v_\perp \sin(-\omega_{ci}t + \pi), \tag{A·2}$$

where $t = 0$ is the time when a particle enters the pulse region. If we define a as $av_\perp = -cE_{y0}/B$, then we have a relation

$$(a+1)v_\perp = v_{sh}, \tag{A·3}$$

because the ion velocity in the upstream region is given by $v_x \simeq -v_{sh}$. When $a = 1$, we have a cycloid motion. Then the integration of the ion current is

$$\int_{\infty}^{x_{wm}} q_i n_w v_{iy} dx \simeq -\int_0^{\pi/\omega_{ci}} q_i n_{w0}(v_x^2 + v_y^2)^{1/2} dt = -Aq_i n_{w0} v_{sh}^2 / < \omega_{ci} > . \tag{A·4}$$

Here, $< \omega_{ci} >$ is the average cyclotron frequency during the integration; thus, roughly, it is given by $< \omega_{ci} > \simeq q_i(B_{wm} + B_{w0})/(2m_i\gamma_0 c)$. The numerical factor A is given by

$$A \simeq \int_{-1}^{1} (1 + a^2 - 2a\xi)^{1/2} d\xi = \frac{(a+1)^3 - |1-a|^3}{3a(a+1)^2}, \tag{A·5}$$

where ξ is introduced by $\xi = \cos(-\omega_{ci}t + \pi)$. The quantity A is 2/3 for $a = 1$ and is 0.96 for $a = 0.5$. Using this, we obtain eq. (30).

1) J. H. Adlam and J. E. Allen: Philos. Mag. **3** (1958) 448.
2) L. Davis, R. Lüst and A. Schlüter: Z. Naturforsch. Teil **A13** (1958) 916.
3) R. Z. Sagdeev: in *Reviews of Plasma Physics*, ed. M.A. Leontovich (Consultants Bureau, New York, 1966), Vol.4, pp.23-91.
4) C.S. Gardner and G.K. Morikawa: Rep. Courant Institute, NYO-9082 (1960).
5) Yu. A. Berezin and V. I. Karpman: Soviet Phys. JETP **46**, 1880 (1964).
6) T. Kakutani, H. Ono, T. Taniuti, and C.C. Wei: J. Phys. Soc. Jpn. **24** (1968) 1159.
7) D. Biskamp, and H. Welter: Nuclear Fusion **12** (1972) 663.
8) D. W. Forslund, K. B. Quest, J. U. Brackbill, and K. Lee: J. Geophys. Res. **89** (1984) 2142.
9) Y. Ohsawa: Phys. Fluids **28** (1985) 2130.
10) R. L. Tokar, S. P. Gary and K. B. Quest: Phys. Fluids **30** (1987) 2569.
11) Y. Ohsawa: Phys. Fluids **29** (1986) 2474.
12) Y. Ohsawa: J. Phys. Soc. Jpn. **55** (1986) 1047.
13) B. Lembege, and J. M. Dawson: Phys. Fluids **B1** (1989) 1001.
14) M. Toida and Y. Ohsawa: J. Phys. Soc. Jpn. **64** (1995) 2036.
15) P. C. Liewer, A. T. Lin, J. M. Dawson, and M. Z. Caponi: Phys. Fluids **24** (1981) 1364.
16) F. de Hoffmann and E. Teller: Phys. Rev. **80** (1950) 692.

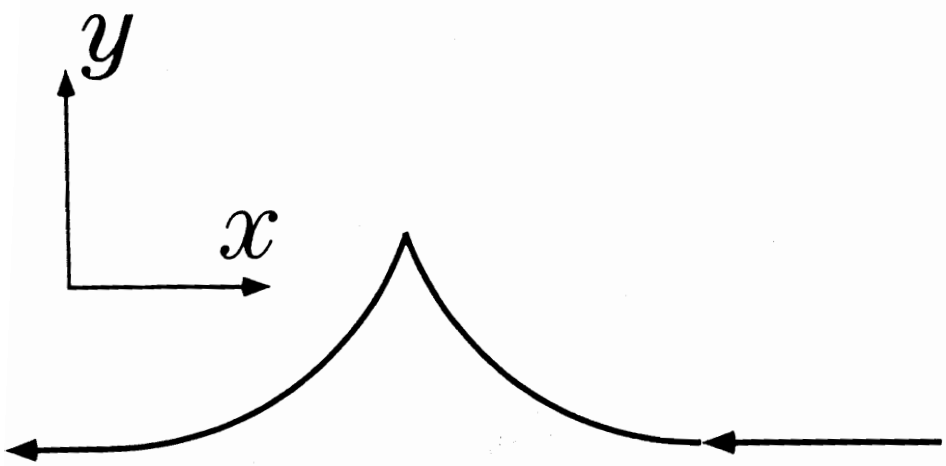
y
x

Fig. 1

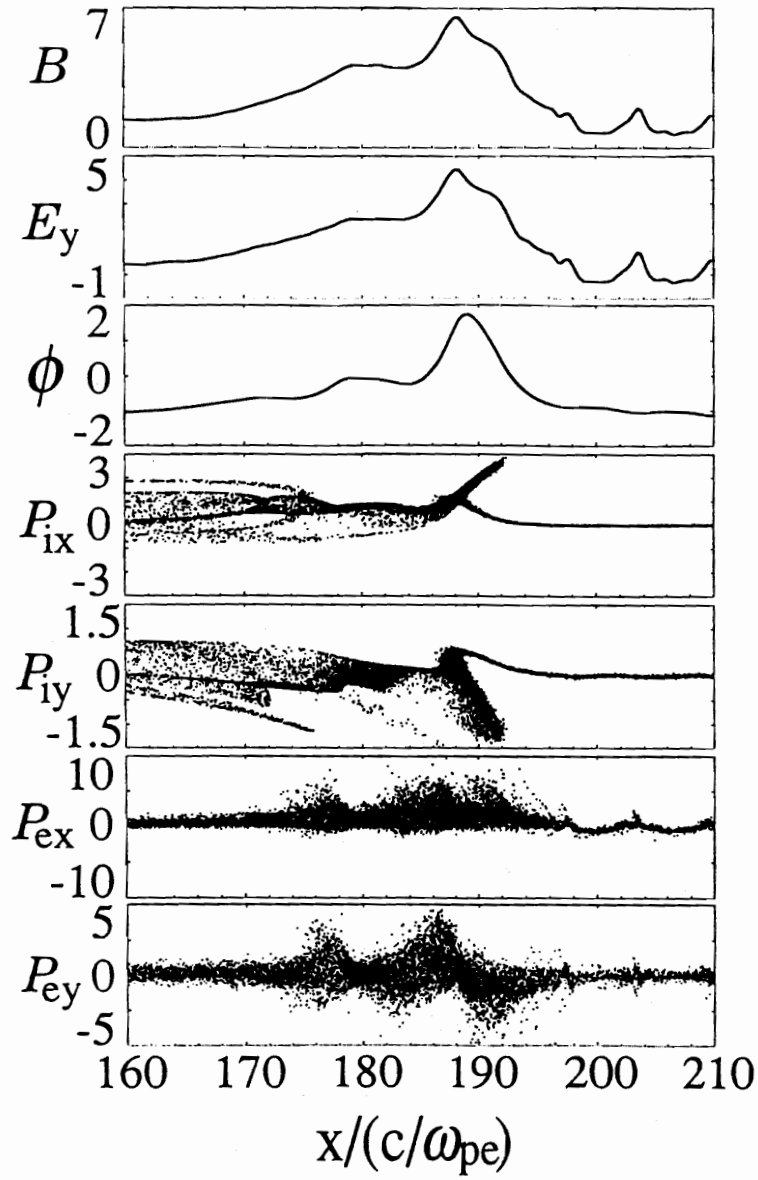
B
7
0
E_y
5
-1
ϕ
2
0
-2
P_{ix}
3
0
-3
P_{iy}
1.5
0
-1.5
P_{ex}
10
0
-10
P_{ey}
5
0
-5
160
170
180
190
200
210
$x/(c/\omega_{pe})$

Fig. 2

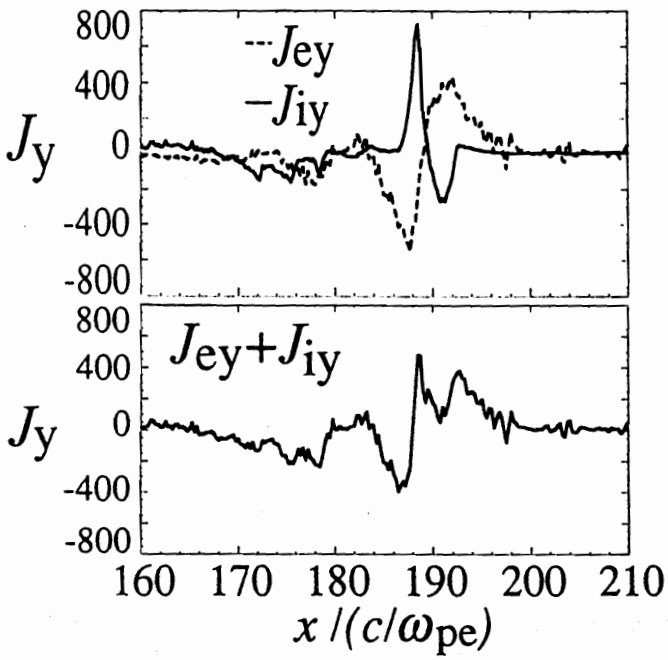
800
400
0
-400
-800
J_y
---J_{ey}
—J_{iy}
800
400
0
-400
-800
J_y
$J_{ey}+J_{iy}$
160 170 180 190 200 210
$x/(c/\omega_{pe})$

Fig. 3

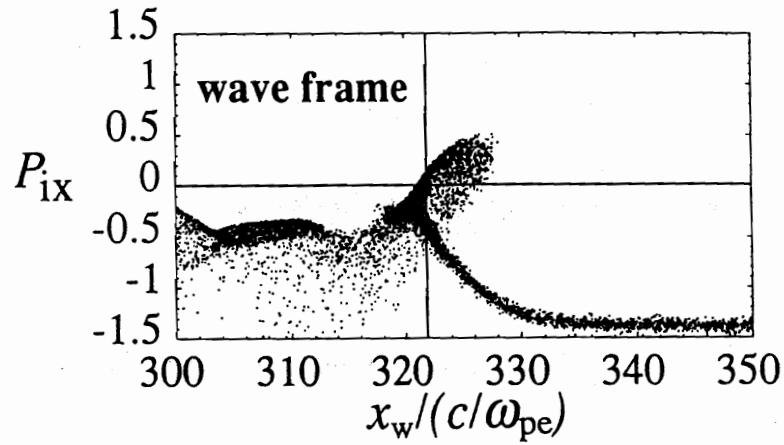
1.5
1
0.5
0
-0.5
-1
-1.5
P_{ix}
wave frame
300 310 320 330 340 350
$x_w/(c/\omega_{pe})$

Fig. 4

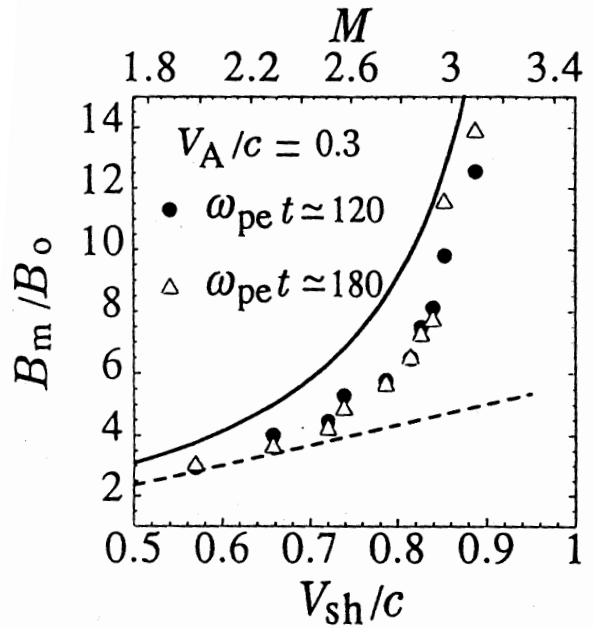
M
1.8 2.2 2.6 3 3.4
$V_A/c = 0.3$
$\omega_{pe}t \simeq 120$
$\omega_{pe}t \simeq 180$
B_m/B_o
V_{sh}/c

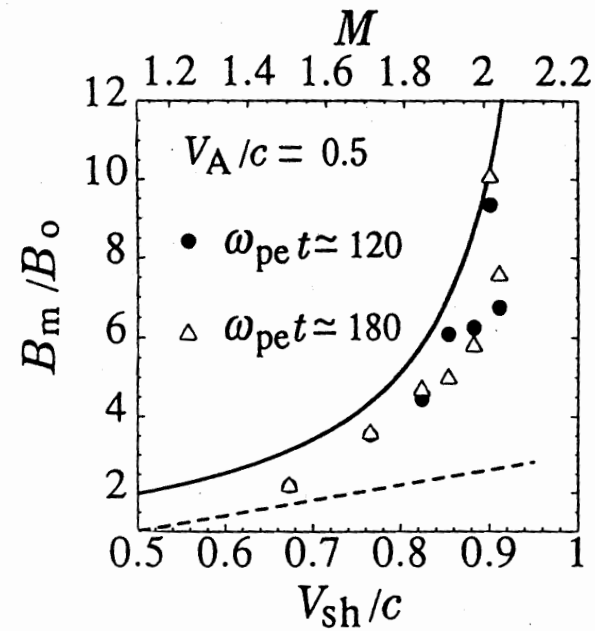
M
1.2 1.4 1.6 1.8 2 2.2
$V_A/c = 0.5$
$\omega_{pe}t \simeq 120$
$\omega_{pe}t \simeq 180$
B_m/B_o
V_{sh}/c

Fig. 5

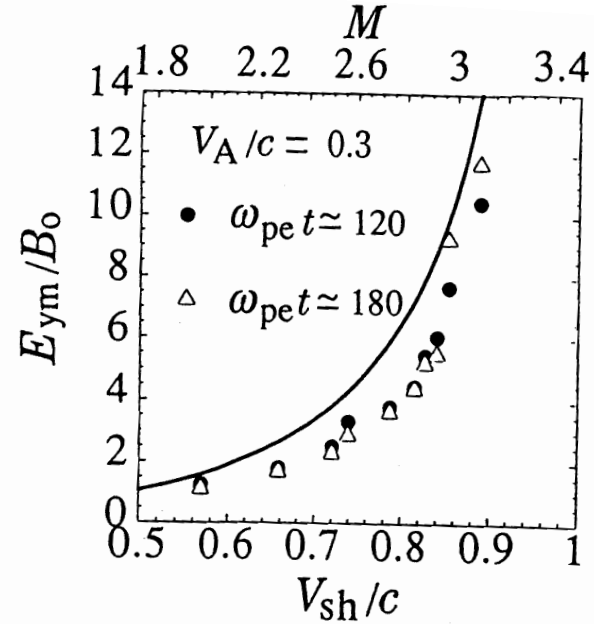
M
1.8 2.2 2.6 3 3.4
$V_A/c = 0.3$
$\omega_{pe}t \simeq 120$
$\omega_{pe}t \simeq 180$
E_{ym}/B_o
V_{sh}/c

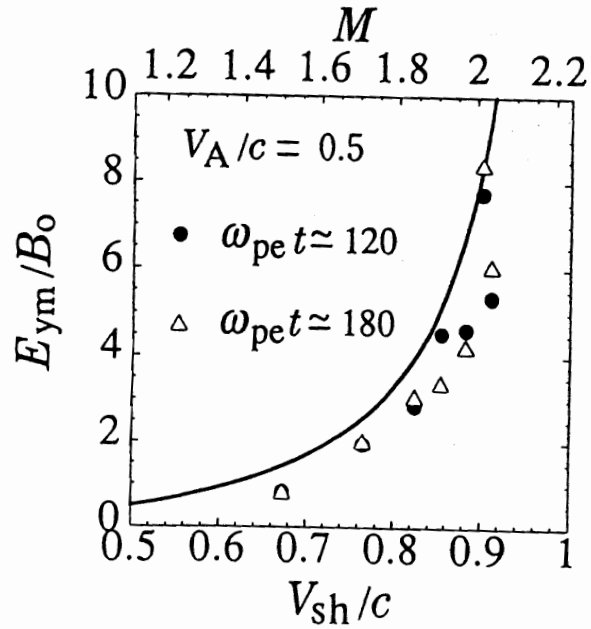
M
1.2 1.4 1.6 1.8 2 2.2
$V_A/c = 0.5$
$\omega_{pe}t \simeq 120$
$\omega_{pe}t \simeq 180$
E_{ym}/B_o
V_{sh}/c

Fig. 6

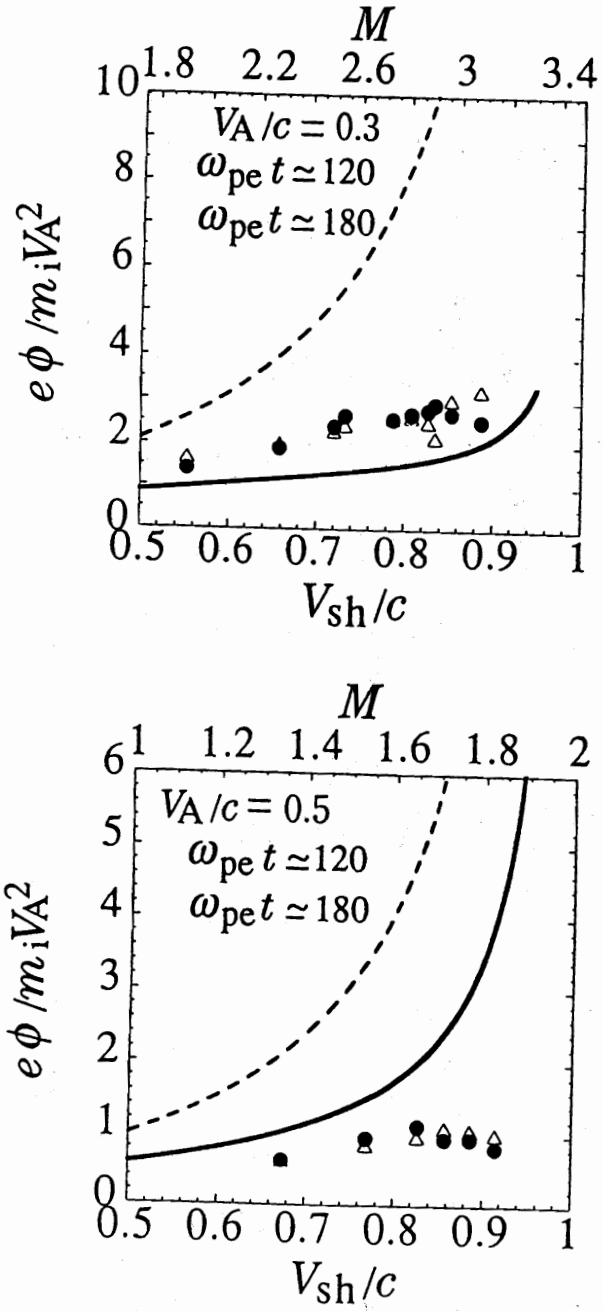
M
1.8 2.2 2.6 3 3.4
$V_A/c = 0.3$
$\omega_{pe}t \simeq 120$
$\omega_{pe}t \simeq 180$
$e\phi/m_iV_A^2$
V_{sh}/c
M
1 1.2 1.4 1.6 1.8 2
$V_A/c = 0.5$
$\omega_{pe}t \simeq 120$
$\omega_{pe}t \simeq 180$
$e\phi/m_iV_A^2$
V_{sh}/c

Fig. 7

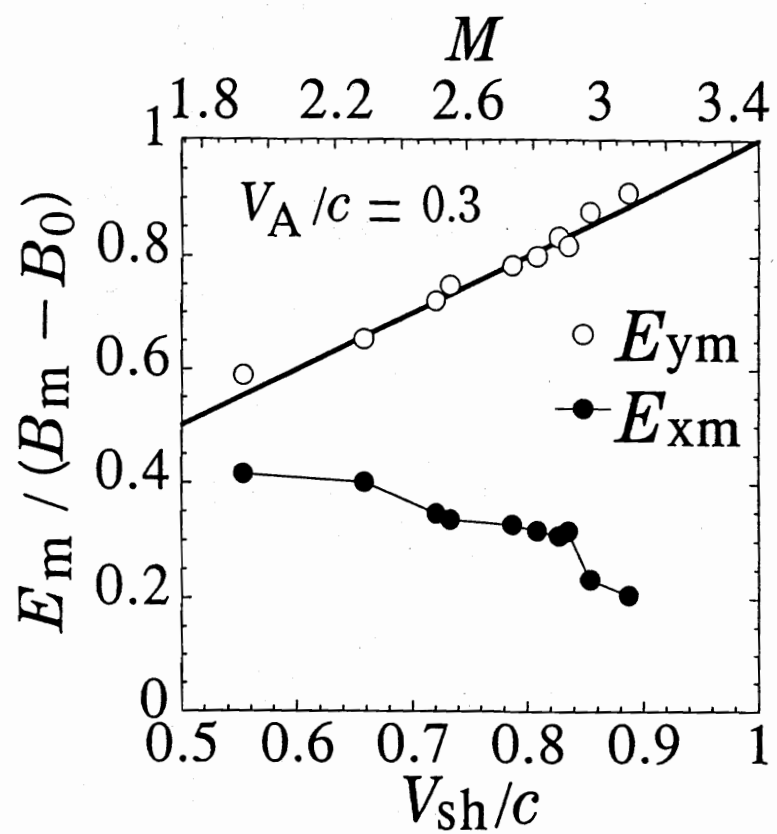
M
1.8 2.2 2.6 3 3.4
$V_A/c = 0.3$
E_{ym}
E_{xm}
$E_m/(B_m - B_0)$
V_{sh}/c

Fig. 8

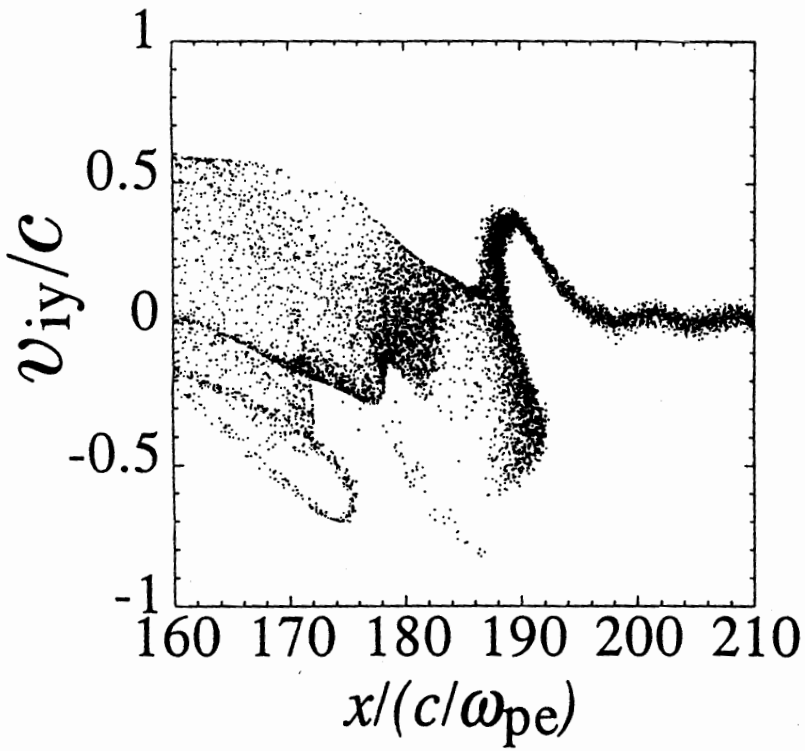

Fig. 9